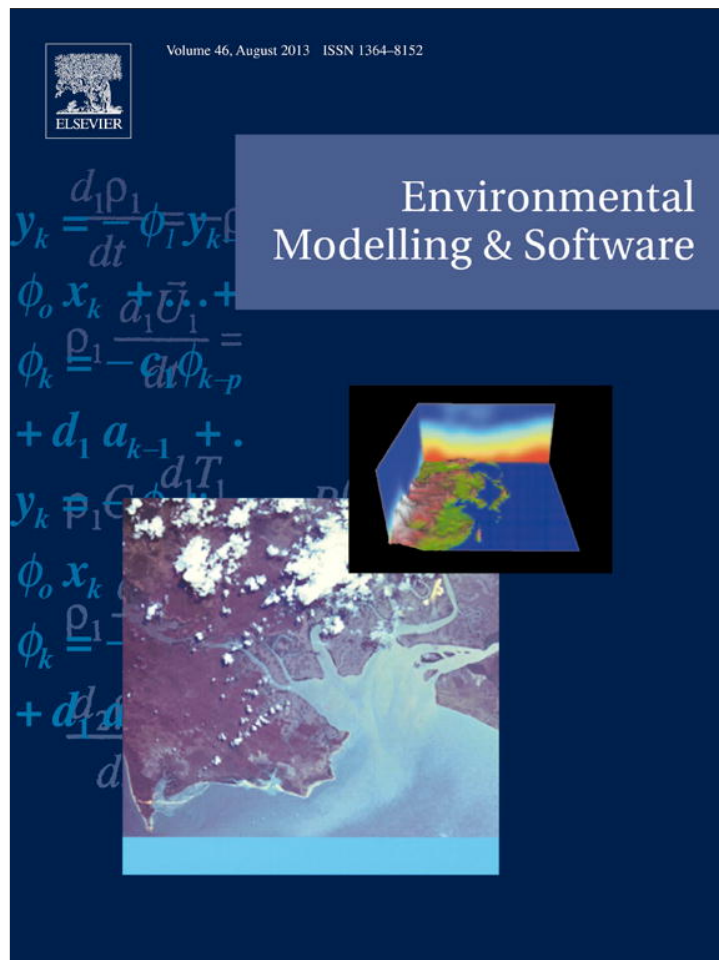


Provided for non-commercial research and education use.  
Not for reproduction, distribution or commercial use.



This article appeared in a journal published by Elsevier. The attached copy is furnished to the author for internal non-commercial research and education use, including for instruction at the authors institution and sharing with colleagues.

Other uses, including reproduction and distribution, or selling or licensing copies, or posting to personal, institutional or third party websites are prohibited.

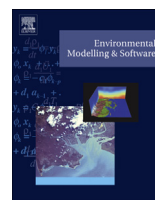
In most cases authors are permitted to post their version of the article (e.g. in Word or Tex form) to their personal website or institutional repository. Authors requiring further information regarding Elsevier's archiving and manuscript policies are encouraged to visit:

<http://www.elsevier.com/authorsrights>



Contents lists available at SciVerse ScienceDirect

## Environmental Modelling &amp; Software

journal homepage: [www.elsevier.com/locate/envsoft](http://www.elsevier.com/locate/envsoft)

# Bridging the scales in a eulerian air quality model to assess megacity export of pollution

G. Siour<sup>a,b,\*</sup>, A. Colette<sup>a</sup>, L. Menut<sup>c</sup>, B. Bessagnet<sup>a</sup>, I. Coll<sup>b</sup>, F. Meleux<sup>a</sup><sup>a</sup> Institut National de l'Environnement Industriel et des Risques, INERIS, 60550 Verneuil en Halatte, France<sup>b</sup> Laboratoire Interuniversitaire des Systèmes Atmosphériques, LISA, Université Paris Est Créteil – Université Paris Diderot, UMR CNRS 7583, 94010 Créteil Cedex, France<sup>c</sup> Laboratoire de Météorologie Dynamique, École Polytechnique, ENS, UPMC, CNRS, IPSL, 91128 Palaiseau, France

## ARTICLE INFO

## Article history:

Received 13 May 2011

Received in revised form

18 March 2013

Accepted 19 April 2013

Available online 18 May 2013

## Keywords:

Chemistry transport modeling

CHIMERE

Stretched grid

Model evaluation

Ozone

Air pollution

## ABSTRACT

In Chemistry Transport Models (CTMs), spatial scale interactions are often represented through off-line coupling between large and small scale models. However, those nested configurations cannot give account of the impact of the local scale on its surroundings. This issue can be critical in areas exposed to air mass recirculation (sea breeze cells) or around regions with sharp pollutant emission gradients (large cities). Such phenomena can still be captured by the mean of adaptive gridding, two-way nesting or using model nudging, but these approaches remain relatively costly. We present here the development and the results of a simple alternative multi-scale approach making use of a horizontal stretched grid, in the Eulerian CTM CHIMERE. This method, called “stretching” or “zooming”, consists in the introduction of local zooms in a single chemistry–transport simulation. It allows bridging online the spatial scales from the city (~1 km resolution) to the continental area (~50 km resolution).

The CHIMERE model was run over a continental European domain, zoomed over the BeNeLux (Belgium, Netherlands and Luxembourg) area. We demonstrate that, compared with one-way nesting, the zooming method allows the expression of a significant feedback of the refined domain towards the large scale: around the city cluster of BeNeLux, NO<sub>2</sub> and O<sub>3</sub> scores are improved. NO<sub>2</sub> variability around BeNeLux is also better accounted for, and the net primary pollutant flux transported back towards BeNeLux is reduced. Although the results could not be validated for ozone over BeNeLux, we show that the zooming approach provides a simple and immediate way to better represent scale interactions within a CTM, and constitutes a useful tool for apprehending the hot topic of megacities within their continental environment.

© 2013 Elsevier Ltd. All rights reserved.

## 1. Introduction

In 2010, there were 20 cities worldwide housing more than 10 million inhabitants, while 30 others had a population exceeding 7 million people (Molina and Molina, 2004; Lawrence et al., 2007). The chemical plumes produced by these megacities contain a large quantity of primary species (NO<sub>x</sub>, volatile organic compounds – VOC, CO and particulate matter – PM) which, at the regional scale, lead to the formation of gaseous oxidants such as ozone as well as organic particulate matter. In addition to their adverse effects on human health (Bell et al., 2006; Gryparis et al., 2004) or ecosystems (Ashmore, 2005; Felzer et al. 2007) and to their contribution to the degradation of regional air quality, many of these compounds

impact the radiative budget of the atmosphere at the global scale (Molina and Molina, 2004; Akimoto, 2003; Crutzen, 2004; Gurjar and Lelieveld, 2005). As a consequence, our ability to quantify the impact of megacities and other emissions hotspots on the composition and long-term evolution of the troposphere constitutes a scientific topic of sustained attention (Chow et al., 2004; Gurjar and Lelieveld, 2005). To address this question, one must be able to track the transport of pollutants originating from megacities, in order to characterize their impacts at multiple temporal and spatial scales.

Several studies have focused on the growing problem of megacities using global (Wild and Akimoto, 2001; Stohl et al., 2002; Lawrence et al., 2007, 2003) and regional (de Foy et al., 2006; Guttikunda et al., 2005) chemistry–transport models. All of them have highlighted the high potential of megacities for affecting the surrounding areas – the amplitude of their impact being strongly dependent on the regional-scale meteorological features prevailing over each individual city. The conclusions all support the

\* Corresponding author. Institut National de l'Environnement Industriel et des Risques, INERIS, 60550 Verneuil en Halatte, France.

E-mail address: [Guillaume.Siour@lisa.u-pec.fr](mailto:Guillaume.Siour@lisa.u-pec.fr) (G. Siour).

importance of bridging local and regional scales when investigating the impact of megacities with Chemical Transport Models (CTM). The study of scale interactions is common to all scientific disciplines and several approaches are used (Voinov and Shugart, 2013; Pisoni et al., 2010; Boumans et al., 2002).

The most widespread approaches to represent the interactions between spatial scales in a CTM are the one-way and two-way nesting methods (Jakobs et al., 1995). One-way nesting consists in using a first broad simulation as initial and boundary conditions for a second simulation of different resolution. It is generally used to constrain, at its boundaries, a high-resolution simulation with the chemical or meteorological fields obtained from a simulation covering a larger domain at lower resolution. In this configuration, both simulations can be computed simultaneously or sequentially, but an important disadvantage of this technique is that there are no possible feedbacks between the small and the large domain. Despite this limitation, this method is widely used and remains appropriate when the impact of the small scale on the larger environment is not the focus of the study (Kaminski et al., 2002). Otherwise, the impact of the small scale the larger scale must be represented. In this case, implementing a two-way nesting approach is more appropriate: the fine and coarse domains are simultaneously simulated so as to allow the exchange of data at each time step of the calculations. This approach is not simple: it requires the elaboration of hypotheses about air mass distribution from large to small grid cells, and deep modifications in the computer code. Indeed, the communication from coarse to fine domains can lead to numerical problems (see Garcia-Menendez and Odman, 2011). Various mesh refinement techniques using structured grids (Srivastava et al., 2000) as well as mesh enrichment techniques on unstructured grids (Tomlin et al., 1997) were thus explored by Garcia-Menendez and Odman (2011). These techniques were developed from simple exercises and designed to prove the worthiness of adaptive gridding in air quality modelling tools, for pollution management purposes. This new type of gridding is promising. However, until now, it was principally used for plume simulation, and it requires further development to be integrated in a CTM.

Alternatively, the feedback of the regional to the larger scale can be represented using a nudging technique. Maurizi et al. (2011) have introduced such a parameterization in the Bolchem CTM (Mircea et al., 2008). This technique consists in nudging a high resolution sub-domain into a low-resolution larger domain. The main advantage of this method is that it allows coupling different models for each scale. However, feedbacks between the coarse and the fine domains cannot all be accounted for.

Stretched grids (also known as “zooming” approaches) are another alternative method. Stretching consists in gradually increasing the horizontal resolution of the model grid over given latitudinal and longitudinal bands. At the intersection of these bands, a grid which is finer than the rest of domain is obtained. Originally, this stretched-grid approach was principally used in weather numerical models, which were successfully used for operational short-term (24–48 h) forecasting (Schmidt, 1977; Staniforth and Mitchell, 1978). It was then introduced in a Global climate model (GCM) by Fox-Rabinovitz et al. (1997) to represent adequately the regional scale over an area of interest. The main interest of this approach resides in its capability to capture real-time feedbacks from the small to the large scale and reversely. The specificity of this technique is that it allows studying the scale interactions without changing the classical structure of CTM.

Our study presents the development and the results of implementing this alternative multiscale approach in the Eulerian CTM CHIMERE. We investigate here its capacity to better apprehend the chemical interactions between a high resolution area and its meso-scale environment. Through this analysis, we aim at evaluating the

benefits of very simple refined gridding processes for the large and for the small domains, compared with classical one-way nesting approaches. In the first part of the paper, we introduce the models used for this study. The methodology that has been developed to bridge the scales in the model is then presented in the second part. Finally, the third part is devoted to a case study analysis.

## 2. Meteorological and chemical models

### 2.1. Description of the CHIMERE chemistry transport model

The CHIMERE model (see the model documentation at <http://www.lmd.polytechnique.fr/chimere/download.php>) uses the reduced MELCHIOR2 chemical mechanism, which is composed of 44 species, including 19 organic species, and 120 reactions. Photolysis rates are calculated under clear sky conditions as a function of height using the TUV model of Madronich et al. (1998). The aerosol module accounts for 14 species (primary particulate matter made of black carbon and organic carbon, but also several biogenic and anthropogenic secondary organic aerosol species – SOA –, sea salts, dust and water) and uses 8 sizes bins from 40 nm to 10  $\mu\text{m}$  (Bessagnet et al., 2005). Dry deposition for gaseous species is parameterized from Wesely (1989) as a downward flux, and a resistance scheme is also included for the aerosols.

Boundary conditions for gaseous species are interpolated from LMDZ-INCA global model data. Anthropogenic emissions are those of the EMEP (<http://www.emep.int/>) inventory which considers  $\text{NO}_x$ , VOC,  $\text{SO}_x$ , CO,  $\text{PM}_{\text{coarse}}$  and  $\text{PM}_{\text{fine}}$  at a resolution of  $0.5^\circ \times 0.5^\circ$ . Biogenic emissions are calculated by the MEGAN model (Guenther et al., 2006).

The horizontal and vertical transport is prescribed by input meteorological fields, processed by the second order Van Leer scheme (Vanleer, 1979).

### 2.2. Description of the WRF mesoscale meteorological model

In this study, the meteorological fields used to drive the CHIMERE CTM are computed with the WRF ARW (Weather research and forecasting) model (Skamarock and Klemp, 2008). This model offers the possibility to perform one-way and two-way nested simulations. For the present study, we have used the two-way nested setup.

From these data, CHIMERE calculates a set of parameters and constrains some physical processes required for chemistry-transport simulations. The planetary boundary layer height is calculated with the Yonsei University scheme (Hu et al., 2010). The convection is parameterized with the Kain-Fritsch scheme (Kain and Fritsch, 1990), and cloud microphysics is described with the WRF Single-Moment 5-class scheme. Long wave and short wave radiations are calculated with the RRTMG scheme (Iacono et al., 2008). The land surface is represented with the RUC Land Surface Model with soil temperature and moisture being given inside six layers, multi-layer snow and frozen soil physics. The surface layer description is based on Monin-Obukhov with Carlson-Boland viscous sub-layer (Skamarock and Klemp, 2008). Finally, both components of the wind ( $u$  and  $v$ ), as well as temperature and specific humidity are nudged towards the large scale NCEP/GFS meteorological reanalyses with a relaxation time scale of 3, 3 and 14 h respectively. This nudging is applied to all vertical levels except in the boundary layer.

## 3. Development of a stretched grid

### 3.1. Technical description

The first step consists in creating an irregular grid from the default CHIMERE grid which uses a plate-carree projection (regular

latitude and longitude grid). The default grid is stretched by applying the following function to the grid resolution over a given area under focus:

$$f = \frac{1}{1 + e^{-i}}$$

where  $i$  is the index of the cell where the resolution starts to increase. This function is normalized and lies between 0 and 1. It is applied to both the latitudinal and longitudinal directions where the spatial resolution  $\Delta\lambda$  follows:

$$\Delta\lambda = \Delta x_{\text{fine}} + (\Delta x_{\text{coarse}} - \Delta x_{\text{fine}}) \times f$$

Thus, the grid spacing decreases over a latitudinal and longitudinal band centred on the area under focus. Using irregular grids in meteorological models raises a number of issues, especially with regards to the propagation of waves (see Fox-Rabinovitz et al., 1997). This is why specific requirements apply to the ratios between the resolutions of neighbouring meshes (Vichnevetsky, 1987; Fox-Rabinovitz et al., 2008 and the references therein). The formulation is less stringent for CTMs, since meteorology is calculated offline and only interpolated or projected on the simulation grid. Consequently, this method can be implemented in a CTM provided that the input data such as meteorology and anthropogenic emissions are consistent with the irregular grid.

### 3.2. Advection of a plume in an academic test case

We conceived an academic case to estimate the geographic effect of grid stretching on the representation of a plume produced by point emissions. A stretched grid was generated with a coarse resolution of  $0.5^\circ$ , gradually decreasing over ten cells to reach the fine resolution of  $0.1^\circ$ , on the latitude band going from  $49.3^\circ\text{N}$  to  $53.6^\circ\text{N}$  (Fig. 1). We simulated the dispersion of a tracer for an ideal case with a constant zonal and meridian wind of  $3 \text{ m s}^{-1}$ , the tracer species being emitted at the point of coordinates ( $51.5^\circ\text{N}$ ,  $5.25^\circ\text{E}$ ) inside the refined area of three simulations. First, a regular coarse simulation at the European scale with a resolution of  $0.5^\circ$ ; second a nested configuration with a high-resolution nested domain located over the Belgium–Netherlands–Luxemburg – BeNeLux – area at a resolution of  $0.1^\circ$  and third a stretched grid also zooming on the BeNeLux area (Fig. 2). The tracer species has a molar mass of  $100 \text{ g mol}^{-1}$  and was emitted continuously during the simulation (120 h), with a total emitted mass of 1000 tons. The vertical profile of the tracer emissions followed a Gaussian curve with a height of 1000 m (sigma: 100 m). Its deposition velocity is the same as for  $\text{NO}_2$ .

The concentration fields of this tracer after 120 h of simulation, extracted around the BeNeLux region at the first level of the model, is presented in Fig. 3 for the three configurations: the regular continental grid of  $0.5^\circ \times 0.5^\circ$  resolution (top left), the regular nested domain of  $0.1^\circ \times 0.1^\circ$  resolution (top right) and the stretched grid with a resolution ranging from  $0.5^\circ$  to  $0.1^\circ$  (bottom left).

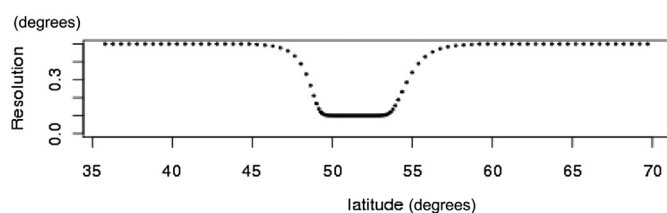


Fig. 1. Horizontal resolution of the stretched grid as a function of latitude, for a given longitude over the European continental domain, with a local zoom on the BeNeLux region.

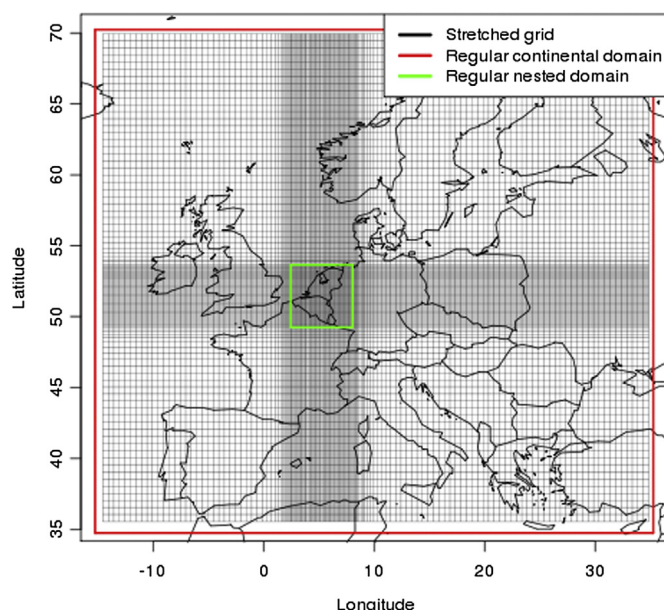
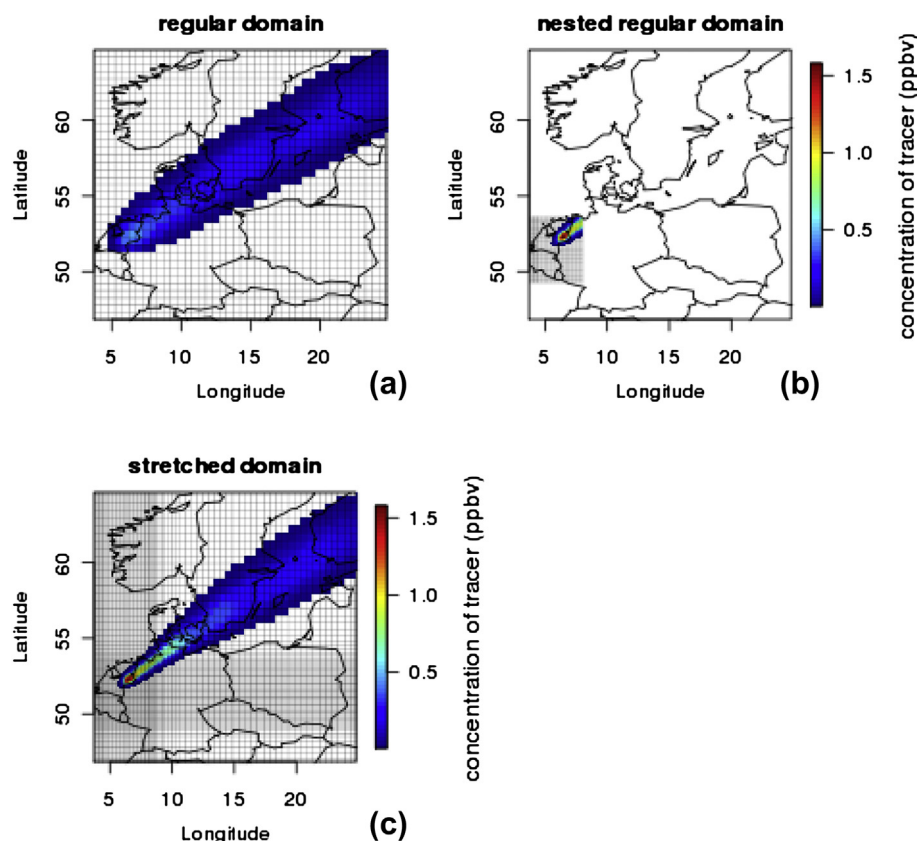


Fig. 2. European stretched grid with a local zoom on the BeNeLux region, with a horizontal resolution ranging from  $0.5^\circ$  to  $0.1^\circ$ . The boundaries of the corresponding domains are represented in red for the continental coarse domain ( $0.5^\circ \times 0.5^\circ$ ), and in green for the fine domain ( $0.1^\circ \times 0.1^\circ$ ).

In all cases, the plume of the inert tracer is transported towards the North-East of Europe, with concentrations logically decreasing away from the emission source. For the nested grid, numerical diffusion is lower: the plume is twice thinner than in the coarse simulation and the tracer plume shows sharper gradients with maximum concentrations being up to 3 times higher. This effect is directly driven by the increase in resolution. Indeed, the same behaviour, with a more detailed structure of the plume, is observed on the stretched grid. However, unlike the nested grid, the stretched grid can capture the intensity and shape of the plume over a larger spatial scale (up to several hundreds of kilometres). Note that we chose in this example to release the tracer in the stretched area. We observed the same tendency with a continental plume coming towards the targeted area: the stretched grid allows better preservation of the imported plume shape while crossing the refined grid.

The major drawback of this method comes from the fact that the grid refinement increases the total number of cells (factor of 2.5 compared with our coarse continental grid), notably over latitudinal and longitudinal bands that are not under focus. Compared with a one-way nested simulation (including both coarse and fine runs), the time increment factor is about 3. This last factor includes the effect of a general decrease in the physical time step for advection calculation, so as to meet the Courant–Friedrichs–Lewy (CFL) condition (Courant et al., 1967). Typically, increasing the resolution by a factor of 5 brings the same multiplying factor on the computational time. Inside our CTM however, this value is calculated from the maximum ratio of wind speed to cell size: if this maximum is not located on the refined part of the grid, the time to satisfy the CFL condition will not always be changed when stretching the grid, limiting the increase in the process time. On the other hand, stretched simulations provide enhanced 2-way information at a lower cost than refined large-scale simulations do. Indeed, our stretched simulation requires a limited number of processors, while simulating a European domain with a resolution of  $0.1^\circ$  may require the use of supercomputers with many processors, with a computational time that increases by an order of



**Fig. 3.** Modelled concentrations (in ppbv) of an inert tracer after 120 h of simulation in an academic meteorological situation with zonal and meridian winds of  $3 \text{ m s}^{-1}$ : (a) regular grid of  $0.5^\circ \times 0.5^\circ$  resolution, (b) nested regular domain of  $0.1^\circ \times 0.1^\circ$  resolution, (c) stretched grid with a resolution ranging from  $0.5^\circ$  to  $0.1^\circ$ . The concentrations are extracted from the first level of the model.

magnitude compared with a continental grid of  $0.5^\circ \times 0.5^\circ$  resolution in the same conditions.

Despite the constraints on calculation time, this method provides an interesting frame for studying intense emission spots and particularly those located on coastal areas. Several studies have indeed demonstrated the importance of sea breeze circulation in coastal smog episodes (Clappier et al., 2000; Evtuyugina et al., 2006; Pirovano et al., 2007). Inside these areas, it is thus important to have a fine representation of meteorology and chemistry to correctly simulate sea breeze recirculation and its impacts on air pollution and ozone production (Mangia et al., 2010), so as to provide a better representation of polluted air mass composition, when they are transported towards the larger scale. Bridging online the spatial scales from the city ( $\sim 1 \text{ km}$  resolution) to the continental area should permit a better representation of pollutant impact from air quality to global change issues.

## 4. Application to a real test case

### 4.1. Simulation period

Summer 2003 was the hottest summer ever experienced over the last fifty years in Europe. The maximum recorded temperatures were significantly higher ( $+2^\circ \text{C}$ ) than during the three hottest summers of this period (1976, 1983 and 1994). This event arose from a classic summertime meteorological situation in Europe, characterized by a high pressure system centred on Western Europe. Only its duration and intensity were exceptional. These conditions promoted the formation of  $\text{O}_3$  at the regional scale, and

its persistence at the continental scale. In particular, unusually high values of  $\text{O}_3$  concentrations were measured in the BeNeLux region (Vautard et al., 2005). On August 1st, European ozone concentrations remain low to moderate but from the 2nd of August on, ozone concentrations increased and far exceeded the European air quality standards ( $180 \mu\text{g m}^{-3}$ ). Remarkably high values were observed along the Mediterranean coasts, in the Ruhr area, in central Europe, and over the whole French territory. On the 12th of August this event came to an end, the whole polluted air mass being pushed eastward by a cold front coming from the Atlantic Ocean (Vautard et al. 2005).

### 4.2. Geographical scope

For the case study, we defined two regular domains and a stretched domain. These domains have the same vertical resolution with 8 pressure levels from the ground to 500 hPa. The first one is a coarse continental domain covering the whole of Europe ( $15.25^\circ \text{W}$ ,  $35.25^\circ \text{E}$ ,  $34.75^\circ \text{N}$ ,  $70.25^\circ \text{N}$ ) with a resolution of  $0.5^\circ \times 0.5^\circ$ . The second, finer, domain extends over the BeNeLux region and includes a fraction of the Ruhr area ( $2.45^\circ \text{E}$ ,  $8.05^\circ \text{E}$ ,  $49.25^\circ \text{N}$ ,  $53.65^\circ \text{N}$ ). It is associated with a  $0.1^\circ \times 0.1^\circ$  horizontal resolution in order to have a better representation of the main cluster of megacities in Northern Europe. This domain is to be nested in the coarse domain. The fine resolution of  $0.1^\circ$  was identified by Valari and Menut (2008) as an optimum scale for the study of the Paris ozone plume with CHIMERE during this specific 2003 summer period. Although this optimum was defined for a specific region and period, we found it relevant for this study. Finally, the stretched

domain was defined so as to match as closely as possible the resolutions and the extents of the regular grids (Fig. 2). As mentioned before, the zooming process requires the combination of two datasets with different resolutions so as to fit on the stretched grid, for both meteorological and emissions data. This specific forcing is described in the next two paragraphs.

#### 4.3. Anthropogenic emissions inventories

The original EMEP emission data are provided at a resolution of  $0.5^\circ \times 0.5^\circ$ . We downscaled this inventory onto our 3 grids as a function of the land use information, using the GLOBCOVER database at a resolution of 300 m (<http://postel.mediasfrance.org/fr/PROJETS/Pre-operationnels-GMES/GLOBCOVER/>). This top down approach allows us to redistribute EMEP emissions on the CTM grids with a high degree of realism. For illustration purposes, the  $\text{NO}_2$  anthropogenic emissions used for this study are represented in Fig. 4, in molecules  $\text{cm}^{-2} \text{s}^{-1}$  and with a decimal logarithmic scale. On the left, we displayed the emissions on the regular grids (coarse and fine at the top and bottom, respectively). On the right, we showed the emissions distributed on the stretched grid. In the BeNeLux area, the fine regular and the stretched domains logically show the same emission resolution and intensity (from about  $10^7$  molecules  $\text{cm}^{-2} \text{s}^{-1}$  up to about  $10^{11}$  molecules  $\text{cm}^{-2} \text{s}^{-1}$ ). In the remainder of the domain, the intensity of emissions is similar between the stretched and coarse regular grids with maxima around  $10^{11}$  molecules  $\text{cm}^{-2} \text{s}^{-1}$  over megacities such as Paris, London, and over the industrialized and urbanized Po-Valley region.

#### 4.4. Interpolation of the meteorological datasets on the stretched grid

Menut et al. (2005) demonstrated the importance of the meteorological resolution to correctly represent reactive species and plume transport at the regional scale. This is why we insisted on having two meteorological datasets, respectively for the coarse and fine areas of all CHIMERE configurations. These datasets has to be consistent with each other to avoid discontinuity at the interface of the coarse and fine grids. As mentioned above, we used the WRF-model in the two-way nesting configuration. The coarse and fine outputs were used to drive respectively the large and small domains of the one-way CHIMERE simulations. As meteorological forcing fields are obtained with a distinct model that does not offer the possibility to use a stretched grid, a merger of both meteorological outputs was used to force the stretched CHIMERE simulation. In this way, the meteorological fields are calculated at the CTM resolution for every area of the regular and stretched domains.

#### 4.5. Measurement data

In order to assess the benefits of the stretching approach, we compared the model results with air quality data from the AirBase repository (<http://air-climate.eionet.europa.eu/databases/airbase>, European Environment Agency). This database includes air quality monitoring data submitted by 35 participating countries throughout Europe. Several hundreds of stations are available, from which we extracted of  $\text{O}_3$  and  $\text{NO}_2$  hourly data. Hourly values have

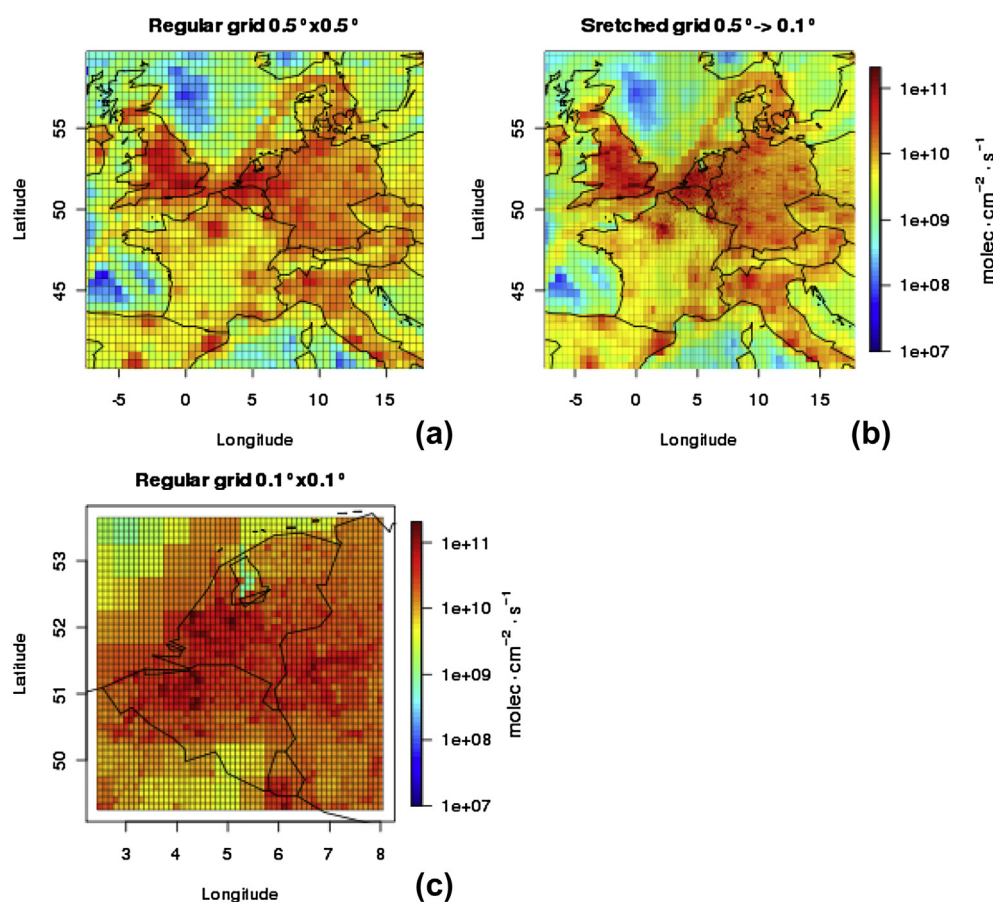
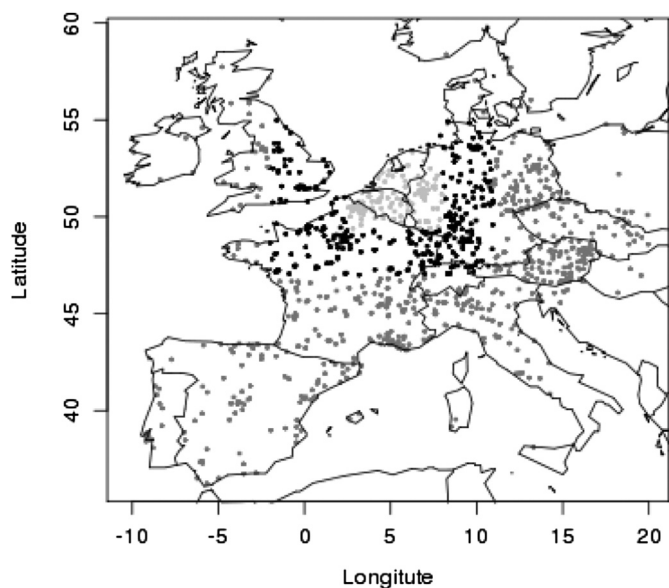


Fig. 4. Surface anthropogenic  $\text{NO}_2$  emissions in molecules  $\text{cm}^{-2} \text{s}^{-1}$  (decimal logarithmic scale): distribution over the (a) regular continental grid, (b) stretched domain and (c) regular small domain.



**Fig. 5.** Location of O<sub>3</sub> “Background” airbase stations: for local validation over BeNeLux (light grey dots, 132 stations), for comparison with ozone around the BeNeLux region (black dots, 360 stations) and for validation at the continental scale (grey dots, 1033 stations).

the advantage of accounting not only for atmospheric levels but also for time evolution along the day, daily variations being an important driver of the intensity of the pollutant chemical transformations. Thus, the correlation between modelled outputs and hourly measurements is a good indicator of model realism. Fig. 5 represents the location of the O<sub>3</sub> airbase stations used in this study. To conduct the analysis, we have defined three measurement subsets:

- in light grey, the stations used for the local validation over the BeNeLux region (131 stations classified as “background” stations and located in different environments: 35 Urban, 45 Rural and 51 Suburban),
- in dark grey the stations used for a validation at the continental scale (1005 background stations: 403 Urban, 328 Rural and 274 Suburban).
- in black, the stations used to validate chemistry and transport at the boundaries of the BeNeLux domain (360 stations: 155 Urban, 93 Rural and 112 Suburban),

The urban/suburban types respectively correspond to stations located in city/in residential areas surrounding cities, which means that they are more influenced by anthropogenic emissions than rural stations that sample cleaner background air. However, all stations are “background” sites, which means that they are always located away from direct source influence (ETC/ACC, 2004).

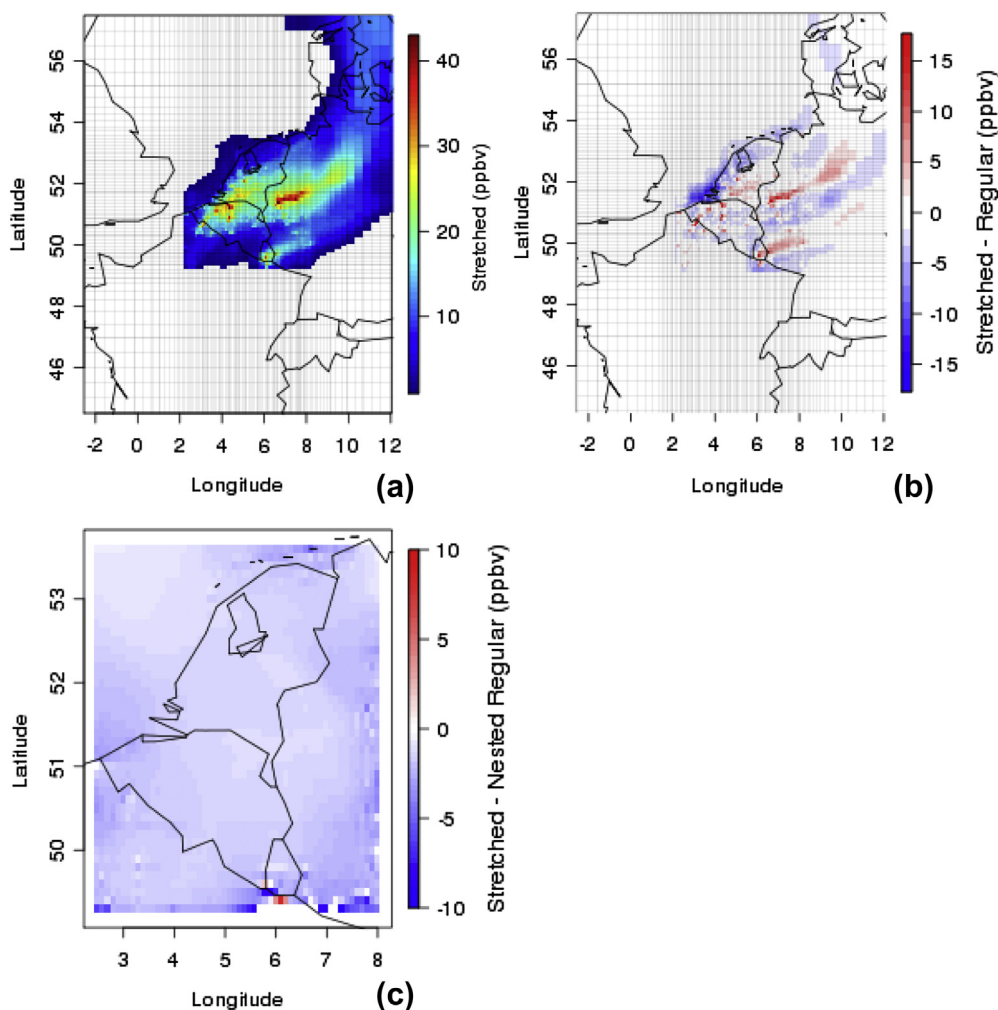


**Fig. 6.** Upper graphs: (a) CO-tracer concentrations at the surface (in ppbv) and (b) differences between the results of the stretched and coarse regular grid configurations (in ppbv) on 2003-07-26 at 2:00 PM. Lower graph (c): mean difference (in ppbv) between the stretched and the nested simulation results over the refined domains, averaged over the whole period.

## 5. Results

### 5.1. Transport of CO from BeNeLux region

Emission tracers are advantageous species for the quantification, in modelling studies, of the impact of an emitter on its environment: they have a unique origin, a reactivity designed for the purpose of the study, and show very sharp gradients due to zero background levels. We introduced such a tracer in the model under the form of a slow-reactive tracer with the same photochemical reactivity as CO, and that was only emitted from the inside of the BeNeLux domain (in both 0.1°-regular and 0.1°-stretched grid configurations, with the same total mass). Its emissions have the same hourly profile and spatial distribution as CO emissions in this area. The upper maps of Fig. 6 represent, on the stretched grid, the concentration of this tracer (on the left) and the difference with the coarse simulation (on the right) for a given day and hour of the simulation period. As expected, we observe that high/low concentration values in the stretched configuration are increased/decreased inside the plumes exported from the BeNeLux region. The concentration gradients are higher (+15ppbv) over hundreds of kilometres in the stretched configuration.

The most interesting results concern the comparison of the stretched grid with the one-way nesting configuration (Fig. 6, lower map): the refined area appears strongly impacted by recirculating tracer plumes from the coarse domain, with negative mean differences [stretched – nested] from –2 to –5 ppbv. Furthermore, there are strong day-to-day variations in this effect, with maximum divergences ranging between –30 and +20 ppbv. These differences cannot be explained by meteorology or emissions which are identical. Only the contribution of continental air masses originating in BeNeLux, and advected back towards this region. Thus, these differences represent the feedback of a better constrained coarse domain on the central refined grid.

### 5.2. NO<sub>x</sub> validation

The changes in pollutant concentration fields brought by the zooming approach have been studied for NO<sub>2</sub>, in order to infer the amplitude of the benefits of this approach for air quality prediction. The two maps of Fig. 7 represent the mean changes in NO<sub>2</sub>

**Table 1**

Model vs observations – scores of NO<sub>2</sub> for all stations of the BeNeLux region: root mean square error and bias.

		RMSE (ppbv)		BIAS (ppbv)	
		Stretched	Regular	Stretched	Regular
BeNeLux region	Mean	12.57	11.65	–1.28	1.59
	Median	10.99	10.55	–0.73	2.56
	Standard deviation	6.63	6.18	10.15	8.27

concentrations from the regular grids (continental and nested) to the stretched one, in ppbv, calculated from 2003-07-31 to 2003-08-13.

When comparing the coarse continental grid with the stretched one (left map), it appears that the main differences are localised inside or around the BeNeLux region with values reaching about –10 ppbv. Over the rest of domain, the concentration fields are quite similar, with null or negligible changes further than 2° from the BeNeLux region. However, strong changes between the 2 configurations are visible along the 2 refined bands of the stretched grid. This was not observed with the CO-tracer, which means that those changes result from the refinement of emissions outside BeNeLux. Thus, not only the zoomed areas, but also surrounding emission areas benefit from the stretched grid refined calculations.

On the right graph, we can see that the mean differences between the stretched configuration and the high resolution nested domain covering BeNeLux are much lower than those observed with the coarse simulation domain. They reach up to 2 ppbv only, as a mean over 15 days. As for the CO-tracer, these divergences account for the supplementary feedback effect of the stretching approach compared with one-way nesting.

We reported in Table 1 the mean and median daily biases as well as the daily root mean square error (RMSE), corresponding to the comparison of modelled with measured NO<sub>2</sub> concentrations in the BeNeLux region. The results show that in this region and in the stretched grid configuration, the model slightly underestimates the observed NO<sub>2</sub> concentrations (with a median bias of –0.73 ppbv), whereas in the nested configuration the model was producing a larger overestimation of NO<sub>2</sub> concentrations with a median bias of 2.56 ppbv compared with measurements. A significant

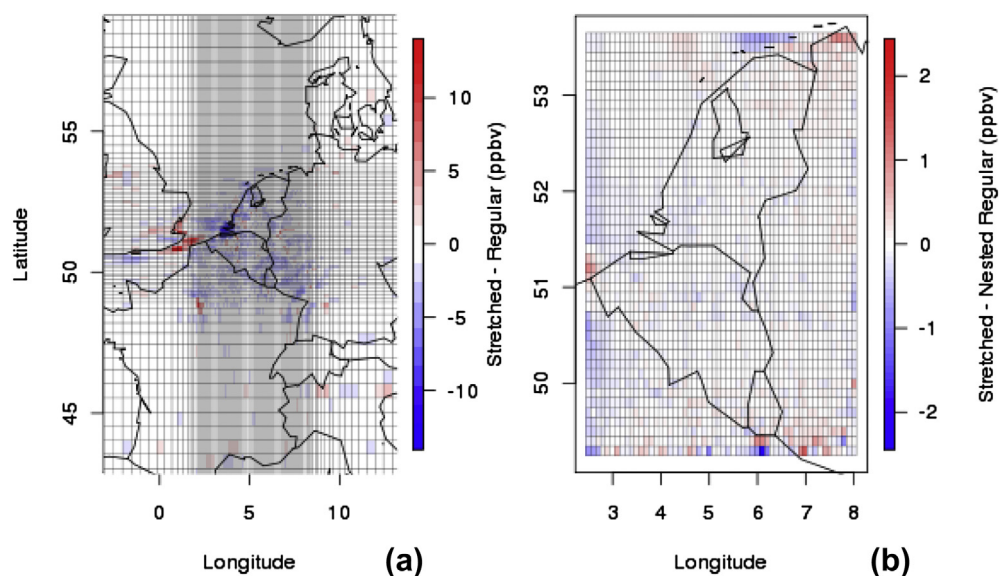


**Fig. 7.** Mean differences in modelled NO<sub>2</sub> concentrations (stretched minus regular configuration, in ppbv) averaged over the period going from 2003-07-31 to 2003-08-13: (a) differences between the stretched and continental regular domains, (b) differences between the stretched and nested domains.

**Table 2**  
Model vs observations – scores of NO<sub>2</sub> around the BeNeLux region, for each type of station: root mean square error and bias.

		RMSE (ppbv)		BIAS (ppbv)	
		Stretched	Regular	Stretched	Regular
Rural	Mean	8.30	8.77	4.04	4.49
	Median	7.47	7.96	3.72	4.22
	Standard deviation	4.88	4.78	5.16	5.25
Suburban	Mean	9.41	9.35	−0.25	−0.62
	Median	8.39	8.42	0.18	0.02
	Standard deviation	5.30	5.07	6.04	5.94
Urban	Mean	11.79	11.84	−4.30	−5.18
	Median	10.83	10.91	−3.81	−4.70
	Standard deviation	5.62	5.58	7.22	7.17

improvement in the restitution of NO<sub>x</sub> concentrations is thus brought by the zooming approach over BeNeLux, compared with one-way nesting.

The same statistical indicators, split onto different background station types (rural, urban, suburban), were calculated over the surroundings of the refined domain. The results of this comparison are given in Table 2. Commonly, little refined air quality model calculations underestimate NO<sub>2</sub> concentrations at urban and suburban stations. Here, the absolute values of the mean RMSE and bias are smaller for the stretched grid compared with the regular domain, in particular along the progressive increase in grid resolution at the surroundings of BeNeLux. It leads to a lower underestimation of mean NO<sub>2</sub> concentrations (−4.30 ppbv for urban sites) compared with the one observed in the coarse simulation (−5.18 ppbv for the same sites). NO<sub>2</sub> being conservative, a decrease is expected in simulated NO<sub>2</sub> concentrations at rural stations compared with the coarse regular grid, as shown in the maps of Fig. 7: the mean and median positive biases of the coarse run are indeed reduced by 11 and 13% in the stretched run. Overall, the stretched grid offers a more realistic representation of NO<sub>2</sub> around the BeNeLux region, originating both in better-defined plumes transported from the BeNeLux and in a refined local calculation, as grid resolution progressively increases close to the targeted area.

### 5.3. Ozone validation

A more accurate representation of primary species concentration fields constitutes a more realistic forcing for secondary pollutant production in the model. We then compared the modelled and observed O<sub>3</sub> concentrations between 2003-07-31 and the 2003-08-13 to assess the improvement in ozone restitution. The daily correlations, bias and RMSE were calculated for each of the 3 areas described in Section 4.5, without discriminating the station types. The median and mean values of RMSE and bias, as well as their standard deviation, are presented in Table 3 for each of

these 3 geographical subsets of stations. Here, for all the computed scores, the “regular” configuration stands for the high-resolution nested area when considering BeNeLux, and for the coarse domain when considering everything but BeNeLux.

At the continental scale, the model correctly reproduces the observed ozone temporal variation, with a median and mean correlation coefficient of 0.84 and 0.74, respectively. These results are consistent with previous CHIMERE evaluations forced with various meteorological models (Honore et al., 2008; Vautard et al., 2006; de Meij et al., 2009). On the stretched grid and at this scale, the correlation is unchanged but the median values of the bias and of the RMSE are improved by 14% and 3% respectively compared with the regular domain.

Around the BeNeLux region, the median and mean of correlation coefficients are either identical or very similar between coarse and stretched configurations. The median bias and RMSE are also slightly improved (20% and 4%, respectively) in the stretched domain run. The ozone concentrations around the targeted region are thus better represented on the stretched grid.

In the BeNeLux area, the median of the correlation coefficients also remains very close (0.89 and 0.90 for the stretched and fine regular grids respectively) but the stretched grid presents a significant increase in ozone overestimation, with a median bias of 8.56 ppbv vs 4.80 ppbv for the regular nested run. As NO<sub>x</sub> concentrations are reduced over the small domain, this overestimation quite probably results from a weaker titration of ozone by nitrogen oxides in the stretched grid. And as the improvement in ozone precursor chemical fields should have carried out improvements in the restitution of secondary pollutant concentration fields. But the atmospheric chemistry is not linear and in a VOC limited regime (high NO<sub>x</sub> emissions) to decrease the NO<sub>x</sub> leading to increase ozone concentrations (McKeen et al., 1991; Liu et al., 1992). In megacity the emissions are very dense and several studies focused on European region (Beekmann and Vautard, 2010) are shown the northwest of Europe as a VOC limited region. If we compared both configurations of our model, a better estimation of NO<sub>x</sub> concentrations with a decrease leads to increase ozone concentrations. In the real world, this increase of ozone production should be compensated by a larger term of deposition, advection or other chemical or physical processes. This is possible than one explanation for the degradation of ozone scores is that we removed error compensation in the ozone production process. In particular, there is a possibility that the model overestimates ozone production in this exceptional meteorological situation (high temperatures with almost no winds and with pollutant accumulation) and that it was partly compensated for by the NO<sub>x</sub> overestimation in the regular grid. One argument that supports this hypothesis is that the differences in simulated ozone concentrations between nested and stretched runs become very close at the end of the event (2003-08-12) when the meteorological situation becomes classic again. Thus,

**Table 3**  
Model vs observations – scores for O<sub>3</sub> for each region: Pearson R coefficient, root mean square error and bias.

		R		RMSE (ppbv)		BIAS (ppbv)	
		Stretched	Regular	Stretched	Regular	Stretched	Regular
The continental domain	Mean	0.74	0.74	19.63	20.14	8.11	9.22
	Median	0.84	0.84	18.66	19.20	7.92	9.04
	Standard deviation	0.29	0.29	8.95	9.23	13.80	13.96
Around BeNeLux region	Mean	0.79	0.80	18.43	18.96	5.59	7.08
	Median	0.87	0.87	17.64	18.32	8.07	9.73
	Standard deviation	0.23	0.23	7.94	8.28	12.43	12.62
BeNeLux region	Mean	0.84	0.85	19.42	16.23	8.24	4.41
	Median	0.89	0.90	17.98	15.12	8.56	4.80
	Standard deviation	0.18	0.17	8.40	6.99	12.18	10.46

**Table 4**

Comparison of the modelled inflow and outflow integrated over the simulation period (2003-07-31–2003-08-13) and over the whole PBL for the BeNeLux region (in  $\mu\text{g m}^{-2} \text{s}^{-1}$ ) for  $\text{NO}_x$  and CO, in the 2 grid configurations.

		$\text{NO}_x$	CO
Stretched grid	Inflow	6.12	555.99
	Outflow	7.74	650.96
	Net flow	-1.62	-94.97
Fine regular grid	Inflow	6.56	569.46
	Outflow	8.05	664.80
	Net flow	-1.49	-95.34
Stretched/Regular	Inflow	0.93	0.98
	Outflow	0.96	0.98
	Net flow	1.09	1.00

the results about primary pollutants, which concentration fields depend on a limited number of processes in the model, may better illustrate the main effect of grid stretching.

5.4. Pollutant fluxes at the boundaries of the BeNeLux region

We calculated the impact of our approach on pollutant transfer across the small domain boundaries. The aim is to evaluate the amplitude of the refinement in the evaluation of net pollutant

fluxes between large cities and their environment. For this purpose, we implemented a calculation of import/export fluxes in CHIMERE.

In a CTM, during each physical time-step, every grid cell communicates with its neighbours in the North, South, West, East, upwards and downwards directions. The import and export fluxes of inert and reactive species around an area of interest can thus be derived from the advection scheme, by calculating the different terms (transport, deposition and production) driving the evolution of all pollutants in the grid. Import/export fluxes (in  $\mu\text{g m}^{-2} \text{s}^{-1}$ ) were computed this way for a virtual domain around the BeNeLux region ( $2.55^\circ\text{E}$ ,  $8.05^\circ\text{E}$ ,  $49.35^\circ\text{N}$ ,  $53.65^\circ\text{N}$ ) from 2003-07-31 to 2003-08-13 and for the whole planetary boundary layer. An integration of the fluxes over the vertical indeed allowed quantifying the total mass transferred to and from the targeted area. These results are given in Table 4 for  $\text{NO}_x$  and CO.

For both  $\text{NO}_x$  and CO, inflows are less important than outflows (a negative net flow represents an export): they derive from the intense urban emissions exported from the BeNeLux. The same net export of  $\text{NO}_x$  was observed by Jakobs and Memmesheimer (2010) who computed comparable horizontal fluxes for a larger domain around BeNeLux during the whole year 2003 with the Eurad model (Hass et al., 1993; Jakobs et al., 1995).

For CO, the net flow is very similar in both model configurations because this species is not very reactive and its budget is little

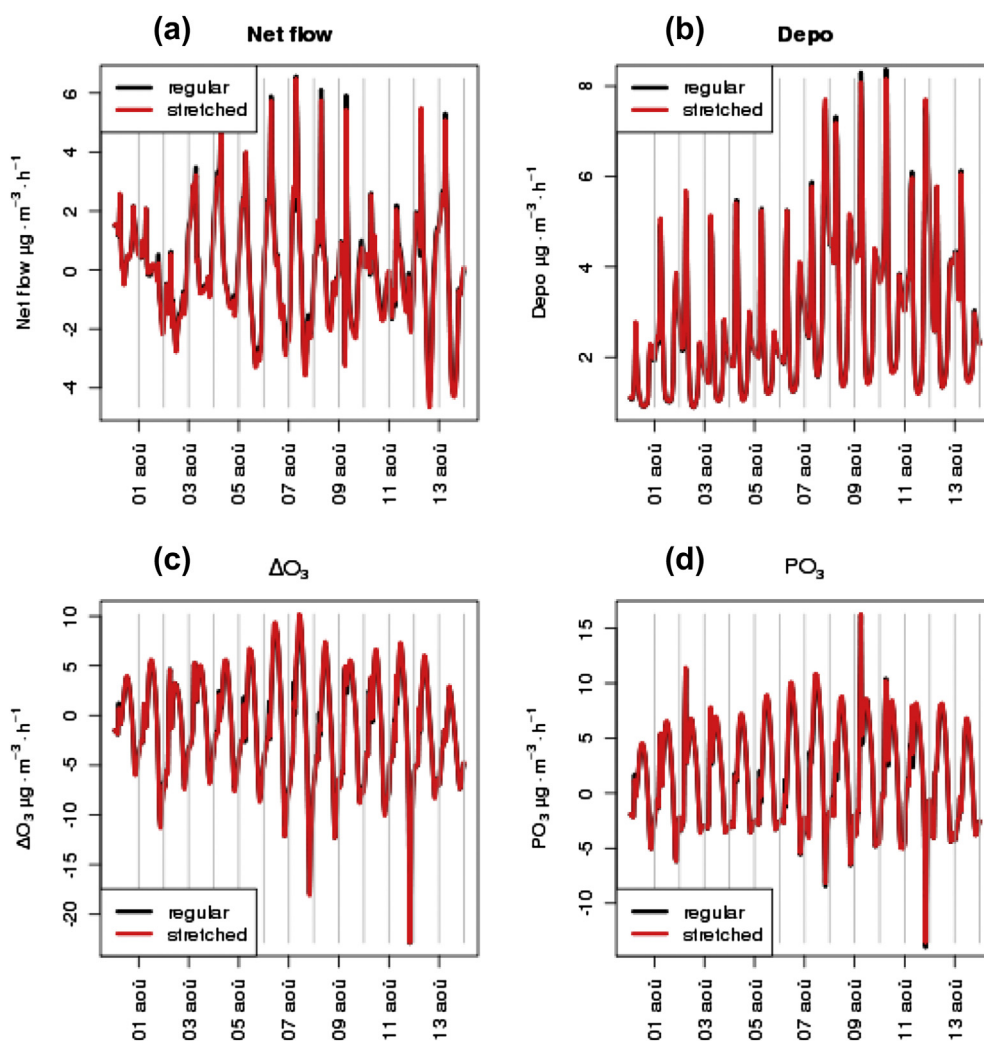


**Fig. 8.** Hourly variation in the modelled processes integrated over BeNeLux and for the planetary boundary layer: (a) net  $\text{O}_3$  pollutant flow, (b) deposition, (c)  $\text{O}_3$  concentration variations ( $\Delta\text{O}_3$ ) and (d)  $\text{O}_3$  production rates ( $\text{PO}_3$ ) in  $\mu\text{g m}^{-3} \text{h}^{-1}$  from 2003-07-31 to 2003-08-13.

sensitive to concentration gradients in the small domain. The inflow and outflow are just slightly reduced (–2%) in the stretched configuration, probably because of the refined representation of emissions at the lateral boundary conditions of BeNeLux.

For more reactive species like  $\text{NO}_x$ , the inflows are reduced by 7% and 4% with the stretched grid. This difference is due to the increased emission resolution around BeNeLux but also to the subsequent change in air mass reactivity, induced by the reinforced concentration gradients in the primary plumes forcing the large domain. Thus, the zooming approach brings significant corrections to the evaluation of fluxes from/to megacities compared with one-way nesting.

### 5.5. Evaluation of ozone production rates

The ozone chemical production rate is a critical issue of air quality management. It is strongly dependent on ozone precursor ratios but also on their absolute concentrations. Thus, it should be affected by grid stretching, which has been shown to modify the  $\text{NO}_x$  peak intensity and concentration distribution. To investigate the impact of modified precursor inflows on ozone, we used the calculated ozone fluxes to compute its production rate in the model. Indeed, the chemical production rate of any pollutant can be deduced from the different terms of the equation of conservation of mass in a grid cell: temporal ozone concentration variation ( $\Delta\text{O}_3$ ), deposition, inflow and outflow, as shown below for ozone.

$$\text{PO}_3(t) = \Delta\text{O}_3(t) + \text{deposition}(t) - \text{flux}_{\text{in}}(t) + \text{flux}_{\text{out}}(t)$$

As photochemistry is more active inside the planetary boundary layer (PBL), we computed and cumulated ozone production rates for every grid cell of the BeNeLux planetary boundary layer. Fig. 8 represents the hourly variation of the net flow, deposition, concentration variation ( $\Delta\text{O}_3$ ) and ozone production given by the above equation in  $\mu\text{g m}^{-3} \text{h}^{-1}$ , from July 31st to August 13th. Both model configurations exhibit very similar variations for each of these processes. The temporal variation of the net ozone flow appears principally driven by meteorology and by ozone concentrations around the area, which are quite similar in the 2 simulations: in the morning, the model calculates a net import (positive values) of ozone due to the PBL height increase, whereas export fluxes dominate (negative value) in the afternoon indicating net and intense ozone production in the PBL. Inferred ozone production rates are maximal between 12 h and 14 h, as it could be expected from the well-known ozone behaviour.

Nevertheless the averaged values of some of these processes, calculated over the whole simulation period (see Table 5) significantly differ in their intensity. As an example, the difference can reach 4% of the mean value for  $\Delta\text{O}_3$ . It can reach a factor of 4 for the net ozone flow, but it is not a major term of the above equation.

**Table 5**

Comparison of mean and median values of the 4 processes calculated over BeNeLux in the 2 configurations: net ozone flow, ozone deposition,  $\text{O}_3$  concentration variation ( $\Delta\text{O}_3$ ) and  $\text{O}_3$  production rate ( $\text{PO}_3$ ) in  $\mu\text{g m}^{-3} \text{h}^{-1}$  averaged over the whole simulation period (2003-07-31–2003-08-13).

		Net flow	Deposition	$\Delta\text{O}_3$	$\text{PO}_3$
Stretched	Mean	–0.09	2.76	–1.33	1.52
	Median	–0.15	2.28	–1.46	1.28
	Standard deviation	1.87	1.56	5.35	4.68
Regular	Mean	0.02	2.75	–1.34	1.39
	Median	–0.09	2.26	–1.53	1.19
	Standard deviation	1.85	1.56	5.18	4.54
Stretched/ Regular	Mean	–3.95	1.00	0.99	1.10
	Median	1.57	1.01	0.96	1.08

These discrepancies result in a mean ozone production rate which is 10% higher in the stretched grid compared with the regular domain. This is the averaged order of magnitude of the impact of small-to-large scale interactions on ozone production rate in the small domain, as can be estimated by a CTM.

## 6. Conclusions

A stretched grid has been implemented in a regional chemistry transport model with the objective of proposing a simple scale-bridging technique that could be used to estimate the impact of megacities and city-clusters on their environment. The method consists in stretching the horizontal resolution of the model grid over given latitudinal and longitudinal bands that meet over an area of interest. Thus, a wide range of spatial scales can be covered within a unique simulation. We showed – for an academic case – that the transport of pollution plumes at the continental scale benefit from the stretching approach, due to a reduced numerical diffusion during advection processes. Then the CHIMERE model was run over Europe for a real case, at a resolution of  $0.5^\circ \times 0.5^\circ$ , in a stretched configuration providing a zoom in resolution over the urban cluster of BeNeLux ( $0.1^\circ \times 0.1^\circ$ ). Particular attention was given to the consistency of spatial scales in the model input data (emissions and meteorology). The results obtained with the stretched grid were compared both with those obtained at a resolution of  $0.5^\circ$  and with a one-way nested simulation focussing on the same urban area, with the same fine resolution. In a second step, all the results were confronted with observations extracted from a European database.

We showed that the zooming technique brings a significant improvement in the restitution of primary pollutant fields around and in the targeted area, compared with techniques only accounting for large-to-small scale interactions. However, this improvement could not be observed over BeNeLux for a complex pollutant such as ozone for which we even observed a degradation of the scores. However, for such complex species submitted to a large number of processes it is very complex to determine the part of error due to grid resolution in the final modelled concentrations, and primary pollutants were considered as better indicators of the benefits of grid refinement. It is finally important to notice that the narrowing of cells along latitudinal bands is clearly responsible for part of the improvement of the model scores at the large scale: it is one of the collateral benefits of the stretched grid principle.

In terms of net species flows between an area of interest and its surroundings, we showed that the stretching approach brings a correction of 5–10% on the transport budget of reactive species such as  $\text{NO}_x$ . The change can reach 10% on integrated ozone production rates, a critical parameter of air quality management studies.

The representation of pollutant emission and transport from a high emitting area remains an essential issue of regional to global air quality and climate change studies. While many studies have demonstrated the need for a better representation of the impact of megacity emissions and chemistry on the larger scale, our study shows that simple gridding approaches may be useful to produce a more realistic view of such scale interactions. It also demonstrates that not only the surroundings of the targeted cities are better constrained by refined gridding but that there also exists significant feedbacks from the large to the small scale. This approach may help taking a first step in the complex issue of the role of large urban areas on tropospheric composition and climate change.

## Acknowledgements

The research leading to these results has received funding from the European Union's Seventh Framework Programme (FP7/2007–

2013) through the CityZen project (Grant Agreement no. 212095). Observation data for this validation were downloaded from the European Air Quality Database (<http://air-climate.eionet.europa.eu/databases/airbase/>). The authors thank the ADEME agency and INERIS for their financial support, Didier Hauglustaine and Sophie Szopa (Institut Pierre-Simon Laplace/LSCE) for the LMDz-INCA data and NOAA's National Weather Service for the NCEP/GFS data.

## References

- Akimoto, H., 2003. Global air quality and pollution. *Science* 302 (5651), 1716–1719.
- Ashmore, M.R., 2005. Assessing the future global impacts of ozone on vegetation. *Plant Cell and Environment* 28 (8), 949–964.
- Bell, M.L., Peng, R.D., Dominici, F., 2006. The exposure–response curve for ozone and risk of mortality and the adequacy of current ozone regulations. *Environmental Health Perspectives* 114 (4), 532–536.
- Bessagnet, B., Hodzic, A., Blanchard, O., Lattuati, M., Le Bihan, O., Marfaing, H., Rouil, L., 2005. Origin of particulate matter pollution episodes in wintertime over the Paris Basin. *Atmospheric Environment* 39 (33), 6159–6174.
- Beekmann, M., Vautard, R., 2010. A modelling study of photochemical regimes over Europe: robustness and variability. *Atmospheric Chemistry and Physics* 10 (20), 10067–10084.
- Boumans, R., Costanza, R., Farley, J., Wilson, M.A., Portela, R., Rotmans, J., Villa, F., Grasso, M., 2002. Modeling the dynamics of the integrated earth system and the value of global ecosystem services using the GUMBO model. *Ecological Economics* 41, 529–560.
- Chow, J.C., Watson, J.G., Shah, J.J., Kiang, C.S., Loh, C., Lev-On, M., Lents, J.M., Molina, M.J., Molina, L.T., 2004. Megacities and atmospheric pollution. *Journal of the Air & Waste Management Association* 54 (10), 1226–1235.
- Clappier, A., Martilli, A., Grossi, P., Thunis, P., Pasi, F., Krueger, B.C., Calpini, B., Graziani, G., van den Bergh, H., 2000. Effect of sea breeze on air pollution in the Greater Athens Area. Part I: numerical simulations and field observations. *Journal of Applied Meteorology* 39 (4), 546–562.
- Courant, R., Friedrich, K., Lewy, H., 1967. On partial difference equations of mathematical physics. *IBM Journal of Research and Development* 11 (2), 215.
- Crutzen, P.J.P., 2004. New directions: the growing urban heat and pollution “island” effect – impact on chemistry and climate. *Atmospheric Environment* 38 (21), 3539–3540.
- de Foy, B., Varella, J.R., Molina, L.T., Molina, M.J., 2006. Rapid ventilation of the Mexico City basin and regional fate of the urban plume. *Atmospheric Chemistry and Physics* 6, 2321–2335.
- de Meij, A., Gzella, A., Cuvelier, C., Thunis, P., Bessagnet, B., Vinuesa, J.F., Menut, L., Kelder, H.M., 2009. The impact of MM5 and WRF meteorology over complex terrain on CHIMERE model calculations. *Atmospheric Chemistry and Physics* 9 (17), 6611–6632.
- Evtugina, M.G., Nunes, T., Pio, C., Costa, C.S., 2006. Photochemical pollution under sea breeze conditions, during summer, at the Portuguese West Coast. *Atmospheric Environment* 40 (33), 6277–6293.
- Felzer, B.S., Cronin, T., Reilly, J.M., Melillo, J.M., Wang, X.D., 2007. Impacts of ozone on trees and crops. *Comptes Rendus Geoscience* 339 (11–12), 784–798.
- Fox-Rabinovitz, M., Cote, J., Dugas, B., Deque, M., McGregor, J.L., Belochitski, A., 2008. Stretched-grid model intercomparison project: decadal regional climate simulations with enhanced variable and uniform-resolution GCMs. *Meteorology and Atmospheric Physics* 100 (1–4), 159–177.
- Fox-Rabinovitz, M.S., Stenichkov, G.L., Suarez, M.J., Takacs, L.L., 1997. A finite-difference GCM dynamical core with a variable-resolution stretched grid. *Monthly Weather Review* 125 (11), 2943–2968.
- Garcia-Menendez, F., Odman, M.T., 2011. Adaptive Grid Use in Air Quality Modeling, pp. 484–509.
- Gryparis, A., Forsberg, B., Katsouyanni, K., Analitis, A., Touloumi, G., Schwartz, J., Samoli, E., Medina, S., Anderson, H.R., Niciu, E.M., Wichmann, H.E., Kriz, B., Kosnik, M., Skorkovsky, J., Vonk, J.M., Dortbudak, Z., 2004. Acute effects of ozone on mortality from the “air pollution and health: a European approach” project. *American Journal of Respiratory and Critical Care Medicine* 170 (10), 1080–1087.
- Guenther, A., Karl, T., Harley, P., Wiedinmyer, C., Palmer, P.I., Geron, C., 2006. Estimates of global terrestrial isoprene emissions using MEGAN (model of emissions of gases and aerosols from nature). *Atmospheric Chemistry and Physics* 6, 3181–3210.
- Gurjar, B.R., Lelieveld, J., 2005. New directions: megacities and global change. *Atmospheric Environment* 39 (2), 391–393.
- Guttikunda, S.K., Tang, Y.H., Carmichael, G.R., Kurata, G., Pan, L., Streets, D.G., Woo, J.H., Thongboonchoo, N., Fried, A., 2005. Impacts of Asian megacity emissions on regional air quality during spring 2001. *Journal of Geophysical Research-Atmospheres* 110 (D20).
- Hass, H., Ebel, A., Feldmann, H., Jakobs, H.J., Memmesheimer, M., 1993. Evaluation studies with a regional chemical-transport model (Eurad) using air-quality data from the emep monitoring network. *Atmospheric Environment Part A-General Topics* 27 (6), 867–887.
- Honore, C., Rouil, L., Vautard, R., Beekmann, M., Bessagnet, B., Dufour, A., Eichegaray, C., Flaud, J.M., Malherbe, L., Meleux, F., Menut, L., Martin, D., Peuch, A., Peuch, V.H., Poisson, N., 2008. Predictability of European air quality: assessment of 3 years of operational forecasts and analyses by the PREV'AIR system. *Journal of Geophysical Research-Atmospheres* 113 (D4).
- Hu, X.M., Nielsen-Gammon, J.W., Zhang, F.Q., 2010. Evaluation of three planetary boundary layer schemes in the WRF model. *Journal of Applied Meteorology and Climatology* 49 (9), 1831–1844.
- Iacono, M.J., Delamere, J.S., Mlawer, E.J., Shephard, M.W., Clough, S.A., Collins, W.D., 2008. Radiative forcing by long-lived greenhouse gases: calculations with the AER radiative transfer models. *Journal of Geophysical Research-Atmospheres* 113 (D13).
- Jakobs, H.J., Memmesheimer, M., 2010. 10 Years of Air Quality Forecast for Europe and Selected Regions – Flux Calculations and Trends of Atmospheric Pollutants in the BeNeLux/Rhein-ruhr Area. IWAQFR: Québec, Canada, poster session.
- Jakobs, H.J., Feldmann, H., Hass, H., Memmesheimer, M., 1995. The use of nested models for air-pollution studies – an application of the Eurad model to a Sana episode. *Journal of Applied Meteorology* 34 (6), 1301–1319.
- Kain, J.S., Fritsch, J.M., 1990. A one-dimensional entraining detraining plume model and its application in convective parameterization. *Journal of the Atmospheric Sciences* 47 (23), 2784–2802.
- Kaminski, J.W., Plummer, D.A., Neary, L., McConnell, J.C., Struzewska, J., Loboocki, L., 2002. First application of MC2-AQ to multiscale air quality modelling over Europe. *Physics and Chemistry of the Earth* 27, 1517–1524.
- Lawrence, M.G., Butler, T.M., Steinkamp, J., Gurjar, B.R., Lelieveld, J., 2007. Regional pollution potentials of megacities and other major population centers. *Atmospheric Chemistry and Physics* 7, 3969–3987.
- Lawrence, M.G., von Kuhlmann, R., Salzmann, M., Rasch, P.J., 2003. The balance of effects of deep convective mixing on tropospheric ozone. *Geophysical Research Letters* 30 (18).
- Liu, S.C., Trainer, M., Carroll, M.A., Hübler, G., Montzka, D.D., Norton, R.B., Ridley, B.A., Walega, J.G., Atlas, E.L., Heikes, B.G., Huebert, B.J., Warren, W., 1992. A study of the photochemistry and ozone budget during the Mauna Loa observatory photochemistry experiment. *Journal of Geophysical Research* 97 (D10), 10463–10471.
- Madronich, S., McKenzie, R.L., Bjorn, L.O., Caldwell, M.M., 1998. Changes in biologically active ultraviolet radiation reaching the Earth's surface. *Journal of Photochemistry and Photobiology B-Biology* 46 (1–3), 5–19.
- Mangia, C., Schipa, I., Tanzarella, A., Conte, D., Marra, G.P., Miglietta, M.M., Rizza, U., 2010. A numerical study of the effect of sea breeze circulation on photochemical pollution over a highly industrialized peninsula. *Meteorological Applications* 17 (1), 19–31.
- Maurizi, A., Russo, F., D'Isidoro, M., Tampieri, F., 2011. Nudging technique for scale bridging in air quality/climate atmospheric composition modelling. *Atmospheric Chemistry and Physics Discussion* 11, 17177–17199.
- McKee, S.A., Hsie, E.Y., Trainer, M., Tallamraju, R., Liu, S.C., 1991. A regional model study of the ozone budget in the eastern United States. *Journal of Geophysical Research* 96 (D6), 10809–10845.
- Menut, L., Coll, I., Cautenet, S., 2005. Impact of meteorological data resolution on the forecasted ozone concentrations during the ESCOMPTE IOP2a and IOP2b. *Atmospheric Research* 74 (1–4), 139–159.
- Mircea, M., D'Isidoro, M., Maurizi, A., Vitali, L., Monforti, F., Zanini, G., Tampieri, F., 2008. A comprehensive performance evaluation of the air quality model BOL-CHEM to reproduce the ozone concentrations over Italy. *Atmospheric Environment* 42 (6), 1169–1185.
- Molina, M.J., Molina, L.T., 2004. Megacities and atmospheric pollution. *Journal of the Air & Waste Management Association* 54 (6), 644–680.
- Pirovano, G., Coll, I., Bedogni, M., Alessandrini, S., Costa, M.P., Gabusi, V., Lasry, F., Menut, L., Vautard, R., 2007. On the influence of meteorological input on photochemical modelling of a severe episode over a coastal area. *Atmospheric Environment* 41 (30), 6445–6464.
- Pisoni, E., Carnevale, C., Volta, M., 2010. Sensitivity to spatial resolution of modeling systems designing air quality control policies. *Environmental Modelling & Software* 25, 66–73.
- Schmidt, F., 1977. Variable fine mesh in a spectral global model. *Beitraege zur Physik der Atmosphaere* 50, 211–217.
- Skamarock, W.C., Klemp, J.B., 2008. A time-split nonhydrostatic atmospheric model for weather research and forecasting applications. *Journal of Computational Physics* 227 (7), 3465–3485.
- Srivastava, R.K., McRae, D.S., Odman, M.T., 2000. An adaptive grid algorithm for air-quality modeling. *Journal of Computational Physics* 165 (2), 437–472.
- Staniforth, A.N., Mitchell, H.L., 1978. Variable-resolution finite-element technique for regional forecasting with primitive equations. *Monthly Weather Review* 106 (4), 439–447.
- Stohl, A., Eckhardt, S., Forster, C., James, P., Spichtinger, N., 2002. On the pathways and timescales of intercontinental air pollution transport. *Journal of Geophysical Research-Atmospheres* 107 (D23).
- The European Topic Centre on Air and Climate Change, 2004. Improvement of Classifications European Monitoring Stations for AirBase, a Quality Control. ETC/ACC.
- Tomlin, A., Berzins, M., Ware, J., Smith, J., Pilling, M.J., 1997. On the use of adaptive gridding methods for modelling chemical transport from multi-scale sources. *Atmospheric Environment* 31 (18), 2945–2959.
- Valari, M., Menut, L., 2008. Does an increase in air quality models' resolution bring surface ozone concentrations closer to reality? *Journal of Atmospheric and Oceanic Technology* 25 (11), 1955–1968.

- Vanleer, B., 1979. Towards the ultimate conservative difference scheme. 5. 2nd-order sequel to Godunov's method. *Journal of Computational Physics* 32 (1), 101–136.
- Vautard, R., Honore, C., Beekmann, M., Rouil, L., 2005. Simulation of ozone during the August 2003 heat wave and emission control scenarios. *Atmospheric Environment* 39 (16), 2957–2967.
- Vautard, R., Szopa, S., Beekmann, M., Menut, L., Hauglustaine, D.A., Rouil, L., Roemer, M., 2006. Are decadal anthropogenic emission reductions in Europe consistent with surface ozone observations? *Geophysical Research Letters* 33 (13).
- Voinov, A., Shugart, H.H., 2013. 'Integronsters', integral and integrated modeling. *Environmental Modelling & Software* 39, 149–166.
- Vichnevetsky, R., 1987. Wave-propagation and reflection in irregular grids for hyperbolic-equations. *Applied Numerical Mathematics* 3 (1–2), 133–166.
- Wesely, M.L., 1989. Parameterization of surface resistances to gaseous dry deposition in regional-scale numerical-models. *Atmospheric Environment* 23 (6), 1293–1304.
- Wild, O., Akimoto, H., 2001. Intercontinental transport of ozone and its precursors in a three-dimensional global CTM. *Journal of Geophysical Research-Atmospheres* 106 (D21), 27729–27744.